An inelastic X-ray scattering spectrometer at LNLS

G. Tirao,[a]‡ G. Stutz[a]* and C. Cusatis[b]

[a]Fa.MAF, Universidad Nacional de Córdoba, 5000 Córdoba, Argentina, and [b]LORXI, Departamento de Física, Universidade Federal do Paraná, 81531 Curitiba, PR, Brazil.
E-mail: stutz@famaf.unc.edu.ar

A high-resolution spectrometer aimed at performing experiments of inelastic X-ray scattering by electronic excitations is described. The spectrometer has been installed at the D12A-XRD1 beamline of the National Synchrotron Light Laboratory (LNLS), in Campinas, Brazil. Synchrotron radiation is monochromated to about 6 keV and focused horizontally onto the sample by a sagittally focusing Si(111) double-crystal monochromator in non-dispersive setting. The spectrometer operates in Rowland circle geometry and is based on a focusing Si(333) analyser in near-backdiffraction geometry for energy analysis of inelastically scattered photons. The analyser works at a fixed Bragg angle, so energy transfers are obtained by varying the incident photon energy. A relative energy resolution of the whole spectrometer of $\sim 1.5 \times 10^{-4}$ at 5.93 keV has been achieved. As an example of application, inelastic X-ray scattering by plasmon excitation in polycrystalline Be was measured. Test results demonstrate that inelastic X-ray scattering experiments with eV energy resolution and an acceptable counting rate are feasible at the LNLS when focused on plasmon and particle–hole excitations.

Keywords: X-ray spectrometer; inelastic X-ray scattering; backdiffracting analyser.

1. Introduction

An inelastic X-ray scattering experiment in the regime of low energy and momentum transfer provides information about electronic excitations, both collective (plasmons) and single-particle-like (electron–hole pair excitations), by measuring the double differential scattering cross section as a function of the transferred energy and momentum (Schülke, 1991). In first-order perturbation theory, the cross section is proportional to the so-called dynamic structure factor, which exclusively reflects properties of the scattering electron system. Thus, inelastic X-ray scattering spectroscopy (IXSS) in this scattering regime provides direct experimental access to solid-state effects revealed in electron excitation spectra. Since X-ray spectrometers based on synchrotron radiation sources are available, resonant and non-resonant inelastic X-ray scattering measurements with high energy resolution and, at the same time, with a high signal-to-noise ratio have been feasible. In this way, IXSS has become a well established technique for studying electronic excitations in condensed matter (see, for example, Schülke, 2001; Hämäläinen & Manninen, 2001; Bergmann *et al.*, 2002, and references therein). Furthermore, there are additional reasons which make IXSS a well suited technique for investigating electronic excitations, at least for low-atomic-number materials. On the one hand, owing to the relatively weak electron–photon coupling, spectrum contamination with multiple scattering is negligible and measurements in a broad range of transferred momentum without large loss of intensity are feasible. On the other hand, the large penetration depth of X-rays allows true bulk information to be obtained, and thus clean sample surfaces are not essential. A description of different types of inelastic X-ray scattering experiments and some examples of applications of IXSS have been reviewed by Schülke (1991). A current review of electronic excitations investigated by IXSS can be found by Schülke (2001).

An X-ray spectrometer conceived to measure energy-loss spectra by valence electron excitations should meet two principal experimental requirements: (i) the energy transfer should cover a range of approximately 100 eV in order to be able to scan either the plasmon peak at low momentum transfers or the whole broad electron–hole pair excitation spectrum at larger momentum transfers; (ii) an energy resolution of the order of 1 eV or better should be achieved in order to be able to investigate fine-structure features in particle–hole excitation spectra, induced by solid-state effects, or to determine line widths in collective excitation spectra. It is required that the magnitude of the momentum transfer can be varied between about a few tenths of and a few times the Fermi momentum at metallic samples and measured with a relative momentum transfer resolution of about a few percent (Schülke, 1991). High-resolution energy analysis of the scattered photons can be performed by means of a crystal analyser in near-backdiffraction geometry. The potentiality of the Bragg backscattering from perfect single crystals for achieving even higher energy resolutions ($\sim$1 meV), along with a large angular acceptance of the crystal, was demonstrated by Graeff & Materlik (1982). Several spectrometers based on nearly-backdiffracting crystals have been constructed at different laboratories for high-resolution resonant and non-resonant IXSS by electron excitation (Schülke & Nagasawa, 1984; Berthold *et al.*, 1992; Stojanoff *et al.*, 1992; Kao *et al.*, 1995; Bergmann & Cramer, 1998; Inami *et al.*, 2001) and for ultrahigh-resolution IXSS by phonon excitation (Burkel *et al.*, 1991; Masciovecchio *et al.*, 1996; Schwoerer-Böhning, *et al.*, 1998; Baron *et al.*, 2001). Here we report on the current status of a backdiffracting spectrometer conceived for carrying out IXSS experiments by valence electron excitations at the D12A-XRD1 beamline at the LNLS. Some preliminary results showing the performance of the spectrometer are also presented.

2. Beamline

The spectrometer was installed on the D12A-XRD1 beamline at the LNLS. Although this beamline was conceived for powder and single-crystal diffraction, it was designed to be versatile in order to be able to mount different types of X-ray experiments. A detailed description of this beamline can be found by Cusatis *et al.* (1998). In this section, the principal components of the beamline are briefly described. The whole experimental set-up is sketched in Fig. 1.

The X-ray source is the 1.67 T D12 bending magnet of the 1.37 GeV storage ring of the LNLS. The critical energy of the synchrotron radiation spectrum is 2.08 keV. At the time of the present work, the injected electron beam current was about 120 mA and the beam lifetime was about 12 h.

A vertical-focusing Rh-coated glass mirror of length 750 mm and width 100 mm was placed between the source and the monochromator. The mirror collects the full vertical angular divergence of the synchrotron beam (0.32 mrad for 6 keV photons) and operates in parallel-beam configuration. The convenience of this operation mode resides in reducing the divergence of the synchrotron X-ray beam reaching the monochromator and thus improving the energy resolution. Actually, an exactly parallel beam cannot be achieved because of the finite vertical source (electron beam) size. The grazing angle is about 5 mrad, thus the high-energy cut-off lies at around 15 keV. This

‡ Present address: LORXI, Departamento de Física, Universidade Federal do Paraná, 81531 Curitiba, PR, Brazil.

 DOI: 10.1107/S0909049504010386

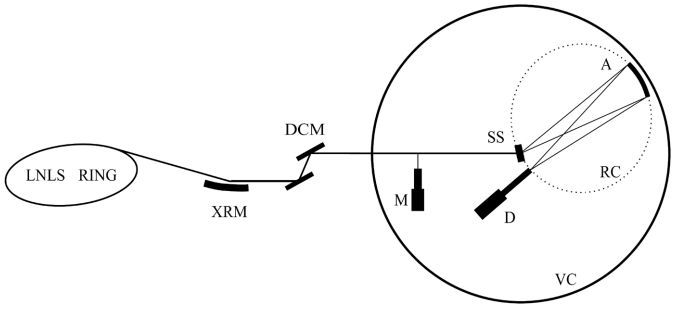

Figure 1
Schematic layout of the experimental set-up at the D12A-XRD1 beamline of the LNLS for inelastic X-ray scattering by electron excitations. XRM: X-ray mirror; DCM: sagittally focusing double-crystal monochromator; M: monitor detector; SS: scattering sample; A: spherically focusing analyser; D: main detector; RC: Rowland circle; VC: vacuum chamber.

value is low enough to eliminate harmonics in the monochromatic beam. The vertical size of the parallel X-ray beam provided by the mirror is about 1.6 mm. A slit system downstream of the monochromator can be used to reduce the beam size should the case arise.

The synchrotron X-ray beam is monochromated by means of a double-crystal Si(111) monochromator in non-dispersive setting. The monochromator design, regarding movement and fine tuning of the crystals, is described elsewhere (Correa *et al.*, 1992). The first crystal is planar and is mounted on a water-cooled copper block in order to remove the thermal load. A liquid InGa contact couples thermally the crystal to the copper block. The second crystal is cylindrically bent in order to sagittally focus the monochromatic beam onto the sample position. About 1 mrad of the horizontal opening angle of the synchrotron beam is collected by the monochromator. The horizontal size of the focused beam at the sample position is about 2.5 mm. The monochromator can be operated in a fixed-exit arrangement, *i.e.* keeping a constant vertical offset between the incident and monochromatic beam.

3. Spectrometer

Energy analysis of the scattered photons is performed by means of a spectrometer consisting of a focusing nearly-backdiffracting crystal analyser in Johann-type arrangement. The spectrometer uses 1:1 Rowland geometry with the scattering sample, as a radiation source, analyser and detector positioned on the Rowland circle (see Fig. 1). The analyser consists of an arrangement of small Si(111) single crystals placed on a spherical surface with a curvature radius of 421 mm. The diameter of the Rowland circle corresponds to the curvature radius of the analyser. The large effective area of the analyser, 8.5 cm in diameter, allows it to collect scattered radiation in a solid angle up to 32 msr. The analyser is mounted on a step-motor-driven two-circle cradle, which allows for a fine angular alignment of the analyser and thus for a precise positioning of the focused beam onto the detector entrance window. The analyser cradle is mounted onto a step-motor-driven vertical goniometer table. The analyser operating at the (333) reflection was positioned at a fixed Bragg angle of 89.2°, thus analysing radiation of 5932.6 eV. The sample holder is mounted onto a rotation axis perpendicular to the analyser table. A goniometer head can be installed as sample holder in order to be able to orient a specific direction of a single-crystal sample with respect to the direction of the momentum transfer. Si pin-diode detectors of active area 7 mm^2 were used as the main and monitor detector. The main detector is mounted on a holder with two translation and two rotation stages, which allows for a rough alignment of the detector at the analyser focalization point. The detector holder is also fixed onto the analyser table. The minimum distance between the sample holder and the detector, together with the analyser curvature radius, determined the analyser Bragg angle of 89.2°, which should be adequate for the present purpose. The whole spectrometer is enclosed in a cylindrical vacuum chamber of diameter 1 m so that the beam path of both incident and scattered photons is in a vacuum (about 0.05 mbar). On the other hand, the dimensions of the scattering chamber constrain the Rowland circle to have a diameter of at most 50 cm (ideally). The flux of the incident beam is monitored registering scattered radiation from a 6.3 μm-thick film of Mylar placed in the path of the incident beam. The scattering plane at the sample and the diffraction plane at the analyser are in the vertical plane. The scattering angle can be continuously varied from 0 to about 150° by rotating the analyser table. Thus, momentum transfers of up to 3 a.u. at 5.93 keV incident energy are accessible, which fulfils the requirements concerning momentum transfer in an IXSS experiment by electronic excitation. The minimum momentum transfer (about 0.1 a.u. for the present spectrometer) is determined by the lowest scattering angle having an acceptable signal-to-background ratio in transmission geometry. The relatively low incident photon energy used by this spectrometer allows inelastic X-ray scattering experiments to be performed with low momentum transfer at scattering angles that are not so small, which are experimentally more easily accessible. As the scattering angle is varied, the whole Rowland circle rotates around the sample axis, and thus the relative position between scatterer, analyser and detector remains unchanged. The benefit of operating the spectrometer in the vertical plane is that measurements for scattering angles close to 90° can be performed without loss of efficiency owing to the polarization-dependent factor of the cross section, since the synchrotron radiation is linearly polarized in the (horizontal) electron orbit plane. Energy-loss scans are accomplished in the so-called inverse geometry, *i.e.* by varying the Bragg angle of the monochromator and by keeping the Bragg angle of the analyser fixed, provided that the cross section varies slowly with the incident energy in the interval of transferred energies of interest (typically less than 100 eV in the scattering regime of valence electron excitation). Changes in the magnitude of the momentum transfer vector owing to variations of the incident photon energy are of the order of 1% or smaller for typical energy transfers.

3.1. Analyser construction and characterization

Different construction procedures have been utilized to obtain spherically bent crystal analysers for IXSS: by gluing and pressing a crystal plate into a concave substrate (Schülke & Nagasawa, 1984; Berthold *et al.*, 1992), by using bending mechanisms (Stojanoff *et al.*, 1992), or by crosswise grooving (Burkel *et al.*, 1991) or dicing (Masciovecchio *et al.*, 1996; Schwoerer-Böhning, *et al.*, 1998) a crystal plate. The latter was applied to build ultrahigh-resolution IXSS spectrometers where the strain appearing by bending can spoil the intrinsic analyser resolution. In the present work, a spherical surface was approximated by positioning about 7800 independent perfect Si single crystals on a spherically ground form. The analyser construction is based on a procedure utilized by the authors previously (Tirao *et al.*, 2002). In this work special attention was paid to diminish the size of the reflecting elements in order to improve the focusing properties of the analyser. This allowed matching of the analyser focus size to the detector active area. The analyser was constructed using a 0.45 mm-thick parallel-faced Si crystal wafer of diameter 100 mm. The wafer surface was parallel to a (111) plane. By dividing the disc into small crystals we benefit from the ability of a Si crystal to

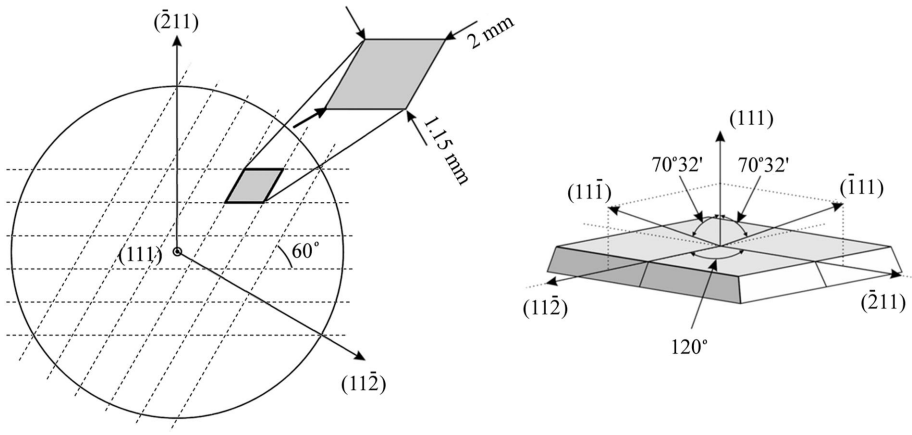

Figure 2
Schematic of the analyser showing the pattern of reflecting elements. Left: the dashed lines indicate the directions along which the wafer surface was scratched. Right: orientation of a single rhombus with respect to some selected crystallographic directions. The cleavage planes are the $(11\bar{1})$ and the $(\bar{1}11)$ planes.

cleave easily along (111) planes. In order to facilitate the cleavage and to obtain small crystals of the same form and size, the wafer surface was scratched using a sharp diamond point along two of the three directions of intersections of the (111) planes with the crystal surface. The surface (111) plane formed angles of 70° 31′ with the other three (111) planes. The lines resulting from the scratching were at a distance of 1 mm from one another in both directions. The angle formed between any two such intersection directions was 60°. Therefore, a pattern of rhombuses with a minor diagonal of 1.15 mm and a main diagonal of 2 mm was obtained (see Fig. 2). Then, the plate was cleaved by pressing it onto a concave surface. Finally, the divided Si wafer was glued and pressed into a glass substrate ground to the appropriate bending radius. Pressure on the wafer was applied by means of a convex teflon form of shorter curvature radius in order to ensure contact in the centre. The teflon form also had a diameter of 100 mm and its flexibility allowed the contact surface to expand progressively from the centre to the border as the pressure was increased. This ensured that the whole segmented wafer made contact with the glass substrate. The teflon form was pushed by a steel cylinder. A high-density rubber sheet between both ensures a uniform distribution of forces applied to the whole crystal surface. A low-viscosity epoxy glue was used, which was cured by exposition to UV light for a few minutes. The relative orientation of the rhombuses was kept unchanged by holding them adhered on an adhesive tape until the glue hardened. Fig. 3 shows an analyser obtained according to the procedure described above.

The original Si wafer was optically polished so that a precise determination of the curvature radius could be easily made using visible light. The measured value was 421 ± 2 mm. The sphericity was checked over the whole analyser surface measuring the curvature radius in different annular sectors. Deviations from the mean value were less than 0.5%, which showed a good uniformity. Focusing properties were also tested using the bremsstrahlung spectrum from a conventional X-ray tube along with a CCD camera as bidimensional position-sensitive detector. The measured radius of curvature was in accordance with that obtained using visible light.

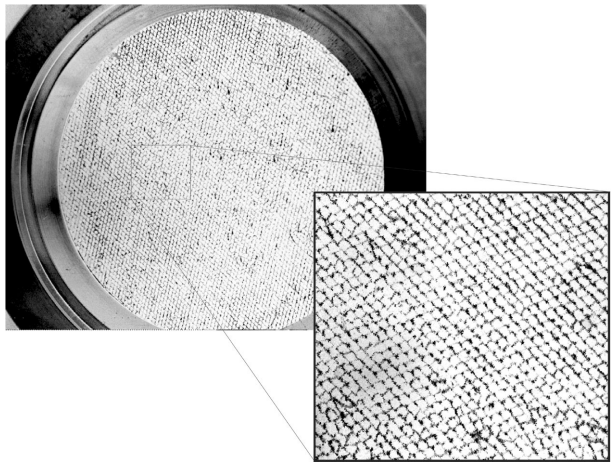

Figure 3
A focusing X-ray analyser mounted on its holder. The enlarged zone of the analyser surface shows the single-crystal reflecting elements in more detail.

3.2. Energy resolution

The relative energy resolution of the whole spectrometer is given by the convolution of the contribution of the monochromator $(\Delta E/E)_{\rm M}$ and that of the analyser $(\Delta E/E)_{\rm A}$,

$$\Delta E/E = \left[(\Delta E/E)^2_{\rm M} + (\Delta E/E)^2_{\rm A}\right]^{1/2}. \quad (1)$$

The monochromator bandpass and the energy resolution of the analyser, measured as the full width at half-maximum (FWHM) of the corresponding energy distribution curves, can be estimated differentiating the Bragg's law and adding quadratically two major contributions,

$$(\Delta E/E)_{\rm M,A} = \left[(\Delta\theta/\tan\theta)^2 + (\Omega/\tan\theta)^2\right]^{1/2}, \quad (2)$$

where the first term of the square root represents the contribution of the deviations of the Bragg angle θ induced by the scattering geometry (geometric term)† and the second term stands for the crystal contribution (intrinsic term). In the latter, Ω describes the FWHM of the two-crystal (single-crystal) reflectivity curve of the monochromator (analyser). This can be well approximated by the angular width of the range of total reflection (Darwin width) (see, for example, James, 1967),

$$\Omega_{\rm D} = 2r_0\lambda^2|F|C/[\pi V\sin(2\theta)], \quad (3)$$

where symmetrical reflection was assumed, r_0 is the classical electron radius, λ is the X-ray wavelength, F is the structure factor, C is the polarization factor [$C = 1$ or $C = |\cos(2\theta)|$ according to whether the polarization vector is perpendicular or parallel to the diffraction plane], V is the volume of the unit cell and θ is the Bragg angle. It is worth noticing that the intrinsic term $(\Omega_{\rm D}/\tan\theta \simeq 1/n^2)$ depends only on the intrinsic properties of the crystal and on the order of the Bragg reflection (n), as long as the energy-dependent dispersion corrections to the atomic scattering factor are not significant. This

† For a divergent beam (spread either along or perpendicular to the diffraction plane) for which the maximum deviation $\Delta\theta$ from the Bragg angle θ of the central ray fulfills $\Delta\theta > \pi/2 - \theta$, and additionally θ is close to 90°, some attention must be paid to evaluate the geometric term. In this particular case, second-order terms in $\Delta\theta$ are to be considered and the geometric term is given by $\Delta E/E|_{\rm geo} \simeq (\pi/2 - \theta)\Delta\theta + 1/2(\Delta\theta)^2 \simeq 1/2(\Delta\theta)^2$ instead of by $\Delta E/E|_{\rm geo} = \Delta\theta/\tan\theta \simeq (\pi/2 - \theta)\Delta\theta$ as indicated in (2).

Table 1
Partial contributions to the relative energy resolution.

	$\Delta E/E \times 10^5$
Monochromator	
Intrinsic	12.4
Geometric	7.4
Total	14.4
Analyser	
Intrinsic	0.8
Geometric	6.8
Beam size (vertical)	5.3
Beam size (horizontal)	0.4
Sample thickness†	2.0
Crystal size (along diffraction plane)	3.8
Crystal size (horizontal)	0.1
Total	6.9
Spectrometer	
Total	16.0

† For the experimental conditions, see text.

suggests that, for a given crystal, high reflection orders are to be used to diminish the crystal contribution. In addition, a Bragg angle as close to 90° as possible is required in order to reduce the geometric term. Setting the analyser to operate at backdiffraction, an increase in the reflection order is necessarily associated with an increase in the energy. In this work, reflections no higher than (333) in Si were employed in order to avoid the large loss of photon flux at energies much higher than the critical energy of the radiation source.

The numerical values of the different contributions of the monochromator and the analyser to the energy resolution are condensed in Table 1. Because of the parallel-beam operation mode of the X-ray mirror, the only geometrical contribution to the energy bandpass of the monochromator is given by the finite size of the electron beam in the vertical direction (0.144 mm FHWM). This introduces a divergence in the white beam impinging on the monochromator of 0.026 mrad, which is one order of magnitude smaller than the FWHM vertical opening angle of the bending-magnet radiation for 5.93 keV energy photons. The calculated energy passband of the monochromator is 0.85 eV at 5.93 keV, which is principally determined by the intrinsic term.

In the case of the analyser, $\Delta\theta$ is mainly given by the convolution of the contributions arising from the finite source size (irradiated volume of the scattering sample) and from the dimensions of the reflecting elements of the spherical analyser. These sources of divergence are treated separately and discussed in detail in Appendix *A*. The divergences introduced by the beam size and by the crystal size in the vertical direction are, in our case, the main contributions to the analyser resolution. The value given in Table 1 for the contribution of the sample thickness corresponds to the experimental conditions used in the test measurements (symmetrical transmission geometry, sample thickness 2.2 mm).

Other geometrical contributions appearing when a Johann-type spectrometer is being used are the Johann aberration and the contribution due to demagnification. The former arises from the fact that only the central point of the crystal surface (bent to a radius R) lies on the focusing circle (of radius $R/2$). The difference in the Bragg angle of the ray impinging on the outer part of the analyser with respect to the central ray can be evaluated from Suortti *et al.* (1999),

$$\Delta\theta = (\Delta\varphi/2)^2/(2\tan\theta), \tag{4}$$

$\Delta\varphi$ being the angular acceptance of the analyser in the diffraction plane, which can be eventually limited by diaphragms. This contribution is at most (for the full analyser opening angle) $\Delta E/E = 0.2 \times 10^{-5}$, which is much smaller than the geometrical contributions listed in Table 1 (except for the horizontal crystal size contribution). The contribution due to demagnification vanishes in the present case because of the use of 1:1 focusing geometry [see, for example, equation (17) of Burkel *et al.* (1991)]. A further contribution due to strain broadening of the reflection curve appearing by spherical bending can be disregarded owing to the use of small flat crystals positioned on a spherical surface.

The theoretical total energy resolution was calculated to be 0.95 eV, which is mainly determined by the monochromator passband.

3.3. Momentum resolution

The transferred momentum resolution is mainly determined by the range of scattering angles $\Delta\phi$ accepted by the angular aperture of the analyser, *via*

$$\Delta q = (E/c)\left|\cos(\phi/2)\right|\Delta\phi, \tag{5}$$

where ϕ is the scattering angle and c is the speed of light. In the derivation of the expression above, energy transfers much smaller than the incident energy E have been assumed. A small analyser aperture results in a good momentum resolution but, on the other hand, a large analyser aperture is desirable in order to collect a large solid angle of scattered radiation. The largest angular aperture is therefore determined by the requirements of momentum resolution of each particular experiment. Usually, circular diaphragms are used to adjust the analyser aperture to the appropriate value. In these particular cases in which the scattered spectrum exhibits no sample-induced anisotropy (polycrystalline or amorphous samples, liquids), one can benefit from the azimuthal isotropy of the scattered radiation around the incidence direction. In these situations, diaphragms with the form of an annular sector as shown in Fig. 4 can be utilized to increase the analyser effective area without degrading the momentum resolution. The radius of the annular sector depends on the scattering angle as $r = L\tan\phi$, L being the distance from the sample to the diaphragm. The height h determines the angular aperture through $\Delta\phi = h/L$. For the present set-up, at the same Δq, an annular diaphragm provides a collected solid angle about 20 (at low ϕ) to 13 (at $\phi \simeq 90°$) times larger than that for a circular diaphragm. Here, diaphragms with $h = 8$ mm placed 402 mm from the sample were considered. The only inconvenience of this type of

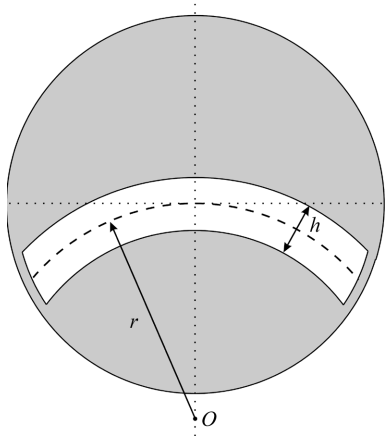

Figure 4
Scheme of an annular diaphragm. r is the radius at the middle of the annular sector of height h. The point O indicates where the transmitted beam passes through.

diaphragm is that for each scattering angle a different diaphragm must be constructed. Diaphragms were 2 mm thick and made of aluminium.

The momentum resolution evaluated from (5) under the above-mentioned conditions is about 0.03 a.u. at low momentum transfers and decreases to 0.01 a.u. at high momentum transfers (3 a.u.). The contribution of the energy bandwidth of the incident beam to the momentum resolution is, depending on the scattering angle, two to three orders of magnitude smaller than the angular contribution.

4. Test measurement

As a performance test, inelastic X-ray scattering in the regime of collective electronic excitation was measured in polycrystalline Be. For plasmon excitation to exist as a dominating excitation mode, the momentum transfer must be $q < q_c$, where $q_c \simeq \omega_p/v_F$ is the plasmon cut-off momentum (Pines, 1964). Here, ω_p is the free electron gas plasmon energy and v_F is the Fermi velocity. At the electronic density of Be the cut-off momentum is $q_c \simeq 0.68$ a.u. Energy-loss spectra at constant $q = 0.44$ a.u. (16° scattering angle) were recorded in inverse geometry. Symmetrical transmission geometry was used. A sample thickness of 2.2 mm was chosen to be close to the mean free path of 6 keV photons in Be in order to optimize the scattering power. Fig. 5 shows the raw data of a typical spectrum. Aside from the elastic line, the inelastic peak due to plasmon excitation can be clearly seen at an energy loss of 20.5 eV. The RPA (random phase approximation) (Pines, 1964) theoretically predicted value of the plasmon energy at $q = 0.44$ a.u. is 21 eV, which is slightly higher than the experimental value. The measured peak position is very close to the values measured by Eisenberger *et al.* (1973) for momentum transfer along the *c* axis and perpendicular to it in h.c.p. Be. Silkin *et al.* (2003) have observed that the RPA plasmon energy in Be for momentum transfers approaching the cut-off momentum is higher than that predicted by their first-principles calculation and those experimentally determined in previous works (Eisenberger *et al.*, 1973; Schülke *et al.*, 1989). A complete set of measurements in Be for different magnitudes of momentum transfer, including the experimental plasmon dispersion and line width obtained with the present spectrometer ,will be presented and discussed in detail elsewhere (Tirao *et al.*, 2004).

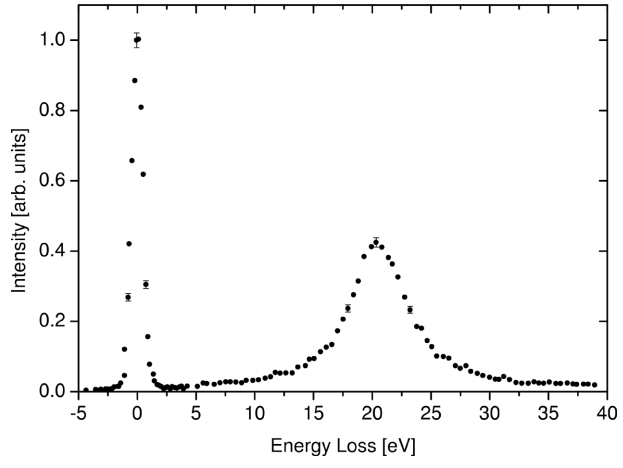

Figure 5
Inelastic X-ray scattering spectrum of polycrystalline beryllium at 0.44 a.u. momentum transfer (16° scattering angle) as a function of the transferred energy. The incident photon energy was scanned around the fixed analyser energy of 5.93 keV. The intensity is normalized to the monitor signal. The counting time for a single data point at the plasmon peak is 30 s.

The total energy resolution of the spectrometer was determined from the width (FWHM) of the elastic line by fitting a Gauss function to the experimental points. From a set of elastic lines, a mean experimental resolution of 1.08 ± 0.07 eV was obtained, which is very close to the calculated value. The difference could be attributed, at least partially, to a non-exact setting of the mirror in the parallel-beam operation mode. The measured counting rate at the maximum of the inelastic peak is 32 counts s^{-1} at a ring current of 100 mA, and the signal-to-background ratio, related to the maximum of the plasmon peak, is better than 75.

5. Summary and conclusions

We have reported a spectrometer designed to perform X-ray energy-loss experiments in the regime of low energy and momentum transfer (valence electron excitations) at the XRD1 beamline of the LNLS. The spectral analysis is made by a spherically focusing multi-single-crystal analyser in near-backdiffraction geometry. The analyser construction is based on a low-cost procedure which consists of dividing a Si plate to approximate a spherical surface, of the appropriate radius, with a large number of small polygons (rhombuses). The whole spectrometer is operated in an evacuated chamber to avoid the absorption of X-rays in air. Test measurements have shown that the achieved energy resolution, counting rate and signal-to-background ratio are very acceptable for carrying out experiments of inelastic X-ray scattering by valence electron excitations in light samples at the LNLS. The measured overall spectrometer resolution is 1.08 eV, which is very close to the calculated value of 0.95 eV. All geometrical effects contributing to the energy resolution were taken into account in the calculation. Further applications of the present spectrometer to experiments such as high-resolution X-ray fluorescence emission (Bergmann *et al.*, 2001) and resonant inelastic X-ray scattering (Hämäläinen & Manninen, 2001) are planned. Concerning the monochromator, focusing properties are expected to be improved, which will allow for collecting a larger horizontal angular divergence of the synchrotron beam and reducing the size of the focused beam at the sample.

APPENDIX *A*
Source and crystal size contributions to the analyser energy resolution

Expressions for the range of Bragg angles ($\Delta\theta$), around the Bragg angle of the central X-ray (θ), corresponding to geometrical effects introduced by the irradiated volume of the sample and by the size of the reflecting elements of the spherical analyser are presented.

A1. Source size contribution

Let us consider a parallel X-ray beam with cross-sectional area of dimensions w_b (horizontal) and h_b (vertical) illuminating a scattering sample of thickness *t*. Horizontal (vertical) direction means a direction perpendicular to the diffraction (orbit) plane. The X-ray beam is scattered by the sample and the energy is analysed by a Johann-type analyser. Both scattering modes (reflection and transmission) in the symmetrical case will be considered. The scattering geometry is illustrated in Fig. 6.

A1.1. Vertical beam size. As can be easily seen in Fig. 6(*a*), the vertical beam size introduces a divergence which, for $h_b \ll R$, is given by

$$\Delta\theta = h_b/(R \sin\theta), \tag{6}$$

where $\Delta\theta$ does not depend on the scattering angle ϕ. It is the goal of symmetrical scattering geometries to allow measuring at different scattering angles, keeping the analyser resolution almost constant. It should be mentioned here that this contribution usually dominates the analyser resolution (see Table 1).

It has been assumed that the vertical detector aperture is larger than $h_b/R\sin\theta$, otherwise the detector size in the vertical direction should appear in (6) instead of h_b. The result above is valid for both scattering geometries.

A1.2. Horizontal beam size. With the help of Fig. 6(*b*), following the relation between θ and the Bragg angle corresponding to the outermost scattered X-ray (θ'), it can be inferred that

$$\sin\theta' = \sin\theta/\left[1 + \left(1/\sin^2\theta\right)(w_b/2R)^2\right]^{1/2}. \quad (7)$$

Writing $\theta' = \theta - \Delta\theta$ and using Taylor expansions up to the second order in $\Delta\theta$ and in w_b/R, one obtains

$$\cos\theta\Delta\theta + [(\sin\theta)/2](\Delta\theta)^2 = [1/(2\sin\theta)] \times (w_b/2R)^2. \quad (8)$$

If $\Delta\theta$ is less than the deviation from perfect backdiffraction ($\Delta\theta < \pi/2 - \theta$), terms of order $(\Delta\theta)^2$ can be neglected and one obtains

$$\Delta\theta = [1/(2\sin\theta\cos\theta)](w_b/2R)^2. \quad (9)$$

On the other hand, if $\pi/2 - \theta < \Delta\theta$ and additionally $\theta \simeq \pi/2$, the approximations $\sin\theta \simeq 1 - 1/2(\pi/2 - \theta)^2$ and $\cos\theta \simeq \pi/2 - \theta$ can be introduced in (8) and the term $(\pi/2 - \theta)\Delta\theta$ can be neglected against $(\Delta\theta)^2$. Then one obtains, for the range of Bragg angles,

$$\Delta\theta = w_b/2R, \quad (10)$$

which gives the expected result at exact backdiffraction.

It has been assumed that the horizontal detector size is larger than the beam size, otherwise w_b should be replaced by the detector dimension in the horizontal direction in (9) and in (10). The expressions derived above do not depend on the scattering geometry.

A1.3. Sample thickness. X-rays scattered at different points of the beam path within the sample will form different Bragg angles with the analyser. The Bragg angle will increase as the incident beam penetrates the sample. The range of Bragg angles, determined by the Bragg angles of the X-rays scattered at the front and at the rear face of the sample, is given by

$$\Delta\theta = t'/(R\sin\theta) = 2t\sin(\phi/2)/(R\sin\theta) \quad (11)$$

for symmetrical transmission and by

$$\Delta\theta = t'/(R\sin\theta) = 2t\cos(\phi/2)/(R\sin\theta) \quad (12)$$

for symmetrical reflection geometry. $t' = 2t\sin(\phi/2)$ [$t' = 2t\cos(\phi/2)$] is the effective

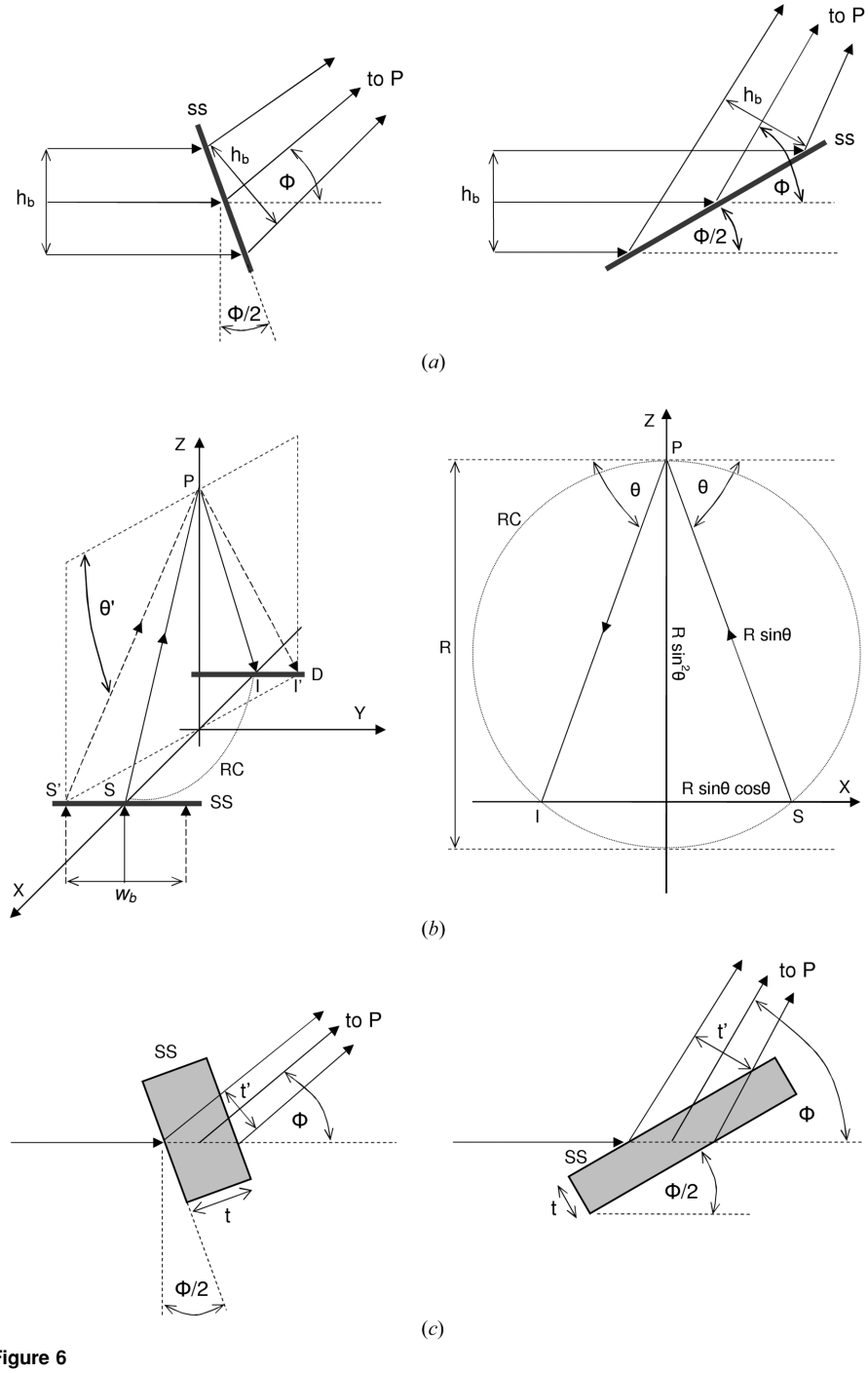

Figure 6
Scheme of the scattering geometry for a parallel X-ray beam of dimensions $w_b \times h_b$ scattered by a sample of thickness t. The scattered beam is analysed by a spherical crystal in Johann geometry. The scattering and the diffraction planes lie on the vertical x–z plane. The orbit plane is parallel to the y–z plane. Source (S), reflection (P) and image (I) points lie on the Rowland circle (RC) of diameter R. $\overline{\mathrm{SPI}}$ ($\overline{\mathrm{S'PI'}}$) displays the path of the central (outer) X-ray. The scattering (Bragg) angle of the central ray is $\phi(\theta)$. SS: scattering sample, D: detector. (*a*) Effect of the vertical beam size on the divergence of the scattered beam. (*b*) Effect of the horizontal beam size on the divergence of the scattered beam. (*c*) Effect of the sample thickness on the divergence of the scattered beam. Symmetrical reflection and transmission scattering geometries are shown separately in (*a*) and (*c*).

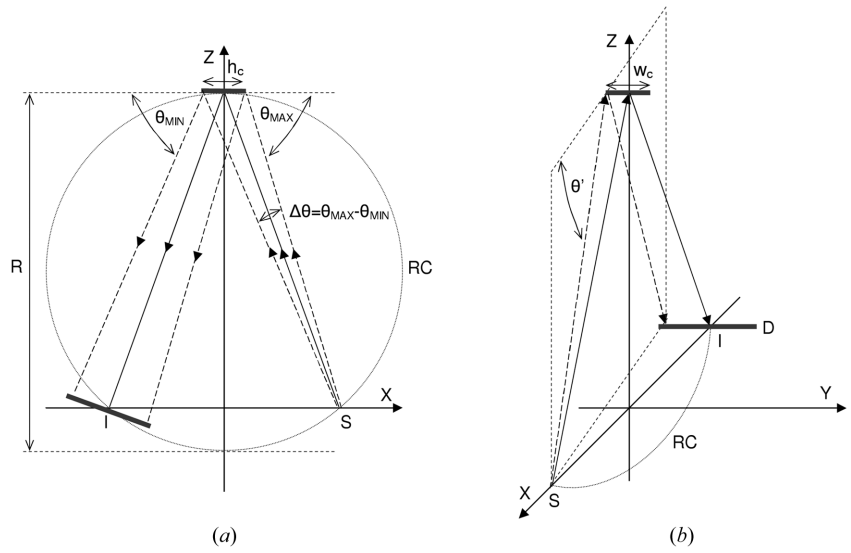

Figure 7
Scheme of the geometry for a polychromatic divergent X-ray beam reflected by a flat crystal of dimensions $w_c \times h_c$. Orientation and symbols as in Fig. 6. (*a*) Effect of the crystal size along the diffraction plane on the angular acceptance of the crystal. (*b*) Effect of the horizontal crystal size on the angular acceptance of the crystal.

height of a finite source originated by a non-zero sample thickness as seen from a point on the analyser for symmetrical transmission [reflection] geometry. For thick samples (namely for thicknesses much larger than the mean free path of the incident X-ray photons), t in (12) should be replaced by the mean free path of the photons, which can be taken as an estimate of the penetration depth. In the case of reflection geometry, it is assumed that thin samples are used (thicknesses smaller than or of the order of the mean free path of the incident X-ray photons). It has been assumed that the vertical angular aperture of the detector is larger than $t'/R\sin\theta$, otherwise the detector size in the vertical direction should appear in (11) and (12) instead of t'.

A2. Crystal size contribution

Let us consider now an analyser consisting of small flat crystals with dimensions w_c (horizontal) and h_c (along the diffraction plane) arranged on a spherical substrate. The horizontal direction is as defined in (Appendix *A*1). The geometrical angular acceptance of the analyser to X-rays scattered from a point in the scattering sample will be determined by the size of the reflecting elements of the analyser. The geometry is illustrated in Fig. 7.

A2.1. Crystal size along the diffraction plane. It is clear from Fig. 7(*a*) that the finite crystal size h_c results in a distribution of Bragg angles. The angular range in the first order of h_c/R can be calculated from

$$\Delta\theta = h_c/R. \tag{13}$$

If the beam size at the detector position ($\sim 2h_c\sin\theta$) is larger than the detector dimension along the diffraction plane (h_d), h_c should be replaced by $h_d/2\sin\theta$ in (13).

A2.2. Horizontal crystal size. A relation between the Bragg angle θ' of the X-ray reflected at a point in the extreme (in the horizontal direction) of a reflecting element and that of the central ray can be inferred from Fig. 7(*b*),

$$\sin\theta' = \sin\theta/\left[1+\left(1/\sin^2\theta\right)(w_c/2R)^2\right]^{1/2}. \tag{14}$$

This expression is the same as that obtained in Appendix *A*1.2, except for the crystal dimension appearing instead of the beam dimension. Proceeding analogously one obtains

$$\Delta\theta = [1/(2\sin\theta\cos\theta)](w_c/2R)^2 \tag{15}$$

for $\Delta\theta < \pi/2-\theta$, and

$$\Delta\theta = w_c/2R \tag{16}$$

for $\pi/2-\theta < \Delta\theta$ and $\theta \simeq \pi/2$.

If the beam size at the detector position ($2w_c$) is larger than the detector size in the horizontal direction (w_d), w_c should be replaced by $w_d/2$ in (15) and (16).

This research was partially supported by the LNLS (National Synchrotron Light Laboratory) and PRONEX/CNPq, Brazil. Financial support from SeCyT (Universidad Nacional de Córdoba) is gratefully acknowledged. The authors thank S. Kycia for helpful discussions and technical assistance at the XRD1 beamline at the LNLS.

References

Baron, A. Q. R., Tanaka, Y., Miwa, D., Ishikawa, D., Mochizuki, T., Takeshita, K., Goto, S., Matsushita, T., Kimura, H., Yamamoto, F. & Ishikawa, T. (2001). *Nucl. Instrum. Methods*, A**467**/**468**, 627–630.
Bergmann, U. & Cramer, S. P. (1998). *Proc. SPIE*, **3448**, 198–209.
Bergmann, U., Glatzel, P. & Cramer, S. P. (2002). *Microchem. J.* **71**, 221–230.
Bergmann, U., Glatzel, P., Robblee, J., Messinger, J., Fernandez, C., Cinco, R., Visser, H., McFarlane, K., Bellacchio, E., Pizarro, S., Sauer, K., Yachandra, V. K., Klein, M., Cox, B. L., Nealson, K. H. & Cramer, S. P. (2001). *J. Synchrotron Rad.* **8**, 199–203.
Berthold, A., Mourikis, S., Schmitz, J. R., Schülke, W. & Schulte–Schrepping, H. (1992). *Nucl. Instrum. Methods*, A**317**, 373–382.
Burkel, E., Dorner, B., Illini, Th. & Peisl, J. (1991). *J. Appl. Cryst.* **24**, 1042–1050.
Correa, M. C., Tolentino, H., Craievich, A. & Cusatis, C. (1992). *Rev. Sci. Instrum.* **63**, 896–898.
Cusatis, C., Kobayashi Franco, M., Kakuno, E., Giles, C., Morelhão, S., Mello, V. Jr & Mazzaro, I. (1998). *J. Synchrotron Rad.* **5**, 491–493.
Eisenberger, P., Platzman, P. M. & Pandy, K. C. (1973). *Phys. Rev. Lett.* **31**, 311–314.
Graeff, W. & Materlik, G. (1982). *Nucl. Instrum. Methods*, **195**, 97–103.
Hämäläinen, K. & Manninen, S. (2001). *J. Phys. Condens. Matter*, **13**, 7539–7555.
Inami, T., Fukuda, T., Mizuki, J., Nakao, H., Matsumura, T., Murakami, Y., Hirota, K. & Endoh, Y. (2001). *Nucl. Instrum. Methods*, A**467**/**468**, 1081–1083.
James, R. W. (1967). *The Optical Principles of the Diffracton of X-rays.* London: G. Bell.
Kao, C.-C., Hamalainen, K., Krisch, M., Siddons, D. P., Oversluizen, T. & Hastings, J. B. (1995). *Rev. Sci. Instrum.* **66**, 1699–1702.
Masciovecchio, C., Bergmann, U., Krisch, M., Ruocco, G., Sette, F. & Verbeni, R. (1996). *Nucl. Instrum. Methods*, B**111**, 181–186.
Pines, D. (1964). *Elementary Excitations in Solids*. New York: W. A. Benjamin.
Schülke, W. (1991). *Handbook on Synchrotron Radiation*, Vol. 3, ch. 15, edited by G. Brown and D. E. Moncton. Amsterdam: Elsevier Science.
Schülke, W. (2001). *J. Phys. Condens. Matter*, **13**, 7557–7591.

Schülke, W. & Nagasawa, H. (1984). *Nucl. Instrum. Methods*, **222**, 203–206.
Schülke, W., Nagasawa, H., Mourikis, S. & Kaprolat, A. (1989). *Phys. Rev. B*, **40**, 12215–12228.
Schwoerer-Böhning, M., Macrander, A. T., Abbamonte, P. & Arms, D. A. (1998). *Rev. Sci. Instrum.* **69**, 3109–3112.
Silkin, V. M., Chulkov, E. V. & Echenique, P. M. (2003). *Phys. Rev. B*, **68**, 205106.
Stojanoff, V., Hämäläinen, K., Siddons, D. P., Hastings, J. B., Berman, L. E., Cramer, S. & Smith, G. (1992). *Rev. Sci. Instrum.* **63**, 1125–1127.
Suortti, P., Buslaps, T., Fajardo, P., Honkimäki, V., Kretzschmer, K., Lienert, U., McCarthy, J. E., Renier, M., Shukla, A., Tschentscher, Th. & Meinander, T. (1999). *J. Synchrotron Rad.* **6**, 69–80.
Tirao, G., Cusatis, C. & Stutz, G. (2002). *X-ray Spectrom.* **31**, 158–161.
Tirao, G., Cusatis, C. & Stutz, G. (2004). To be published.

 Received 18 December 2003 • Accepted 28 April 2004